Journal of Applied Mechanics and Technical Physics, Vol. 49, No. 2, pp. 209–216, 2008

FORMATION MECHANISM OF CAVITATING SPALLS

M. N. Davydov and V. K. Kedrinskii

UDC 532.5.013.2+532.528+534.222

The dynamics of formation of cavitation zones in a liquid upon reflection of a shock pulse from the free surface is studied numerically in a one-dimensional formulation using the Iordanskii–Kogarko–van Wijngaarden two-phase model. It is shown that the formation of a system of cavitation zones (clusters) with a dynamically increasing volume concentration of the gas phase near the free surface is due to oscillations of the structure of the rarefaction wave profile. The fast relaxation of tensile stresses in the cavitation zone ends in the formation of a quasistationary mass-velocity field, which provides for almost unbounded growth of cavitation bubbles in subsurface clusters and explains the occurrence of the spall layers observed in experiments.

Key words: *strength of liquid, dynamic loading, bubble cavitation, spalls.*

Introduction. The problem of liquid breakdown in intense rarefaction waves is directly related to the notion of strength, which does not have a precise and clear definition in the mechanics of liquids under dynamic loading, unlike in solid mechanics. This is due primarily to the fact that real liquids, even in the unperturbed state, contain cavitation nuclei in the form of microheterogeneities of the type of free gas microbubbles, solid microparticles and their combinations [1–3]. The development of cavitation on these nuclei leads to significant changes in the parameters and structure of the external wave field, because of which the notion of critical tensile stresses for liquids is not defined.

Nevertheless, in some experimental studies (see, for example, [4, 5]), the occurrence of a mass-velocity jump on a free liquid surface upon reflection of the shock pulse from it is treated as a manifestation of spall type fracture. In this case, according to the data of [4], the value of the spall strength is determined from the formula $p_s = 0.5\rho_0 c_0(W_0 - W_{\min})$ and depends on the velocity jump $W_0 - W_{\min}$ (W_0 is the maximum velocity of the free surface at the moment of reflection and $W_{\min}$ is its minimum value which is recorded before the spall pulse).

In [5], based on experimental results on the behavior of the free surface of a water layer, it is concluded that the quantity p_s is almost constant and varies in the range 38–42 MPa, depending on loading methods. However, this conclusion is not unambiguous because it does not follow from the results of [5] for the smallest values of the strain rate $\dot{\varepsilon} = (2.0\text{–}2.7)\cdot 10^4$ sec^{-1} obtained at $p_0 = 40$ MPa and $p_0 = 1050$ MPa. In particular, in the case $p_0 = 40$ MPa, the spall strength $p_s > 38$ MPa, i.e., close to the amplitude of the initiating shock pulse. Consequently, the energy of the shock pulse is not consumed in spall formation or the spall strength is much smaller than the value indicated above. We note that, in [4], the occurrence of spalling in a metal sample under shock-wave loading is explained by features of the free-surface dynamics recorded experimentally. The same approach was used in [4, 5] to describe the behavior of liquids under similar loading conditions.

As noted above, there is no direct analogy between the fracture processes of liquids and solids does not exist, and this refers, first of all, to the concept of critical tensile stresses. The conclusion that shock loading of a liquid results in the occurrence of a spall pulse [4, 5] is only an interpretation of the recorded jump of the free surface velocity $W(t)$, and the fact of spalling requires experimental support.

The unusual response of the free surface to the initiating pressure pulse was found in [6], where the Iordanskii–Kogarko–van Wijngaarden (IKW) model was used in a numerical analysis of the nonstationary stage of rarefaction-

Lavrent'ev Institute of Hydrodynamics, Siberian Division, Russian Academy of Sciences, Novosibirsk 630090; davydov@hydro.nsc.ru; kedr@hydro.nsc.ru. Translated from Prikladnaya Mekhanika i Tekhnicheskaya Fizika, Vol. 49, No. 2, pp. 65–73, March–April, 2008. Original article submitted March 26, 2007.

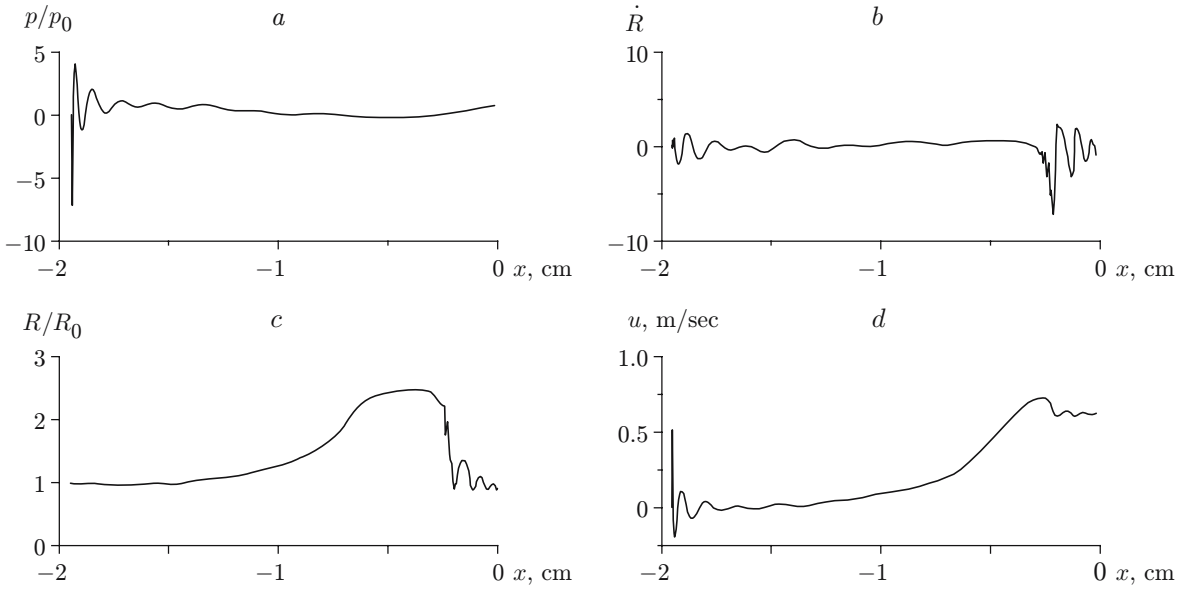

Fig. 1. Distributions of the pressure (a), radial velocity of cavitation bubbles (b), their radii (c), and mass velocity (d) in the nonstationary stage of decay of an arbitrary discontinuity in a hydrodynamic rarefaction tube ($t = 13$ μsec).

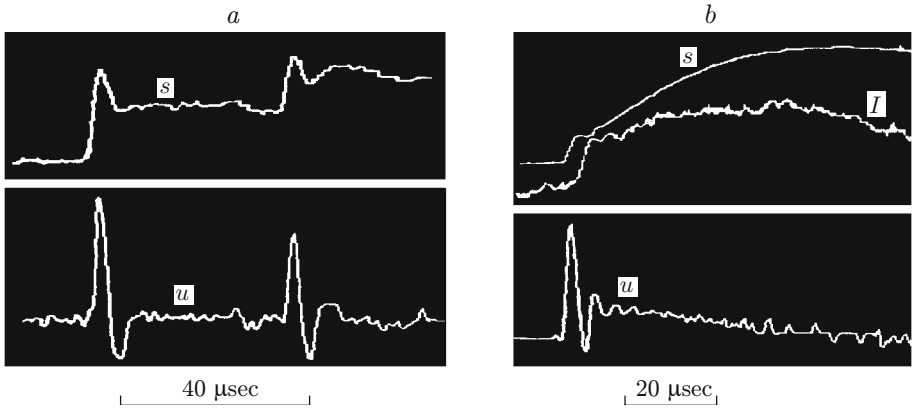

Fig. 2. Dynamics of the free-surface displacement s and its mass velocity u: (a) precavitation regime; (b) intense development of cavitation leading to the occurrence of a velocity jump.

wave formation in the problem of decay of an arbitrary discontinuity during rupture of a diaphragm in a hydrodynamic rarefaction tube which separates a high-pressure chamber with a liquid layer from the atmosphere (Fig. 1). The coordinate $x = 0$ corresponds to the free surface of the liquid layer. The calculation showed that the time of response of the surface was much larger than the loading time. One clearly see a step in the curve of mass-velocity distribution $u(x)$ near the free surface (Fig. 1). An analysis showed that this jump was a response of the surface to the development of a cavitation zone near it.

An experimental study of this phenomenon was performed in [7]. The displacement s of the surface due to the reflection of a shock wave from it was measured by a capacitive transducer, and the mass velocity u was determined as the derivative of the displacement (Fig. 2). The velocity profile u agrees with an oscillogram of the incident ultrashort ($\tau \approx 5$ μsec) pressure pulse with a rarefaction phase which was generated by the motion of the diaphragm of an electromagnetic hydrodynamic shock tube under the action of a pulsed magnetic field. The oscillograms in Fig. 2a correspond to the pre-cavitation regime. The spike corresponding to the wave reflected from the membrane is evident in Fig. 2a. The oscillograms in Fig. 2b were obtained at the stage of developed cavitation:

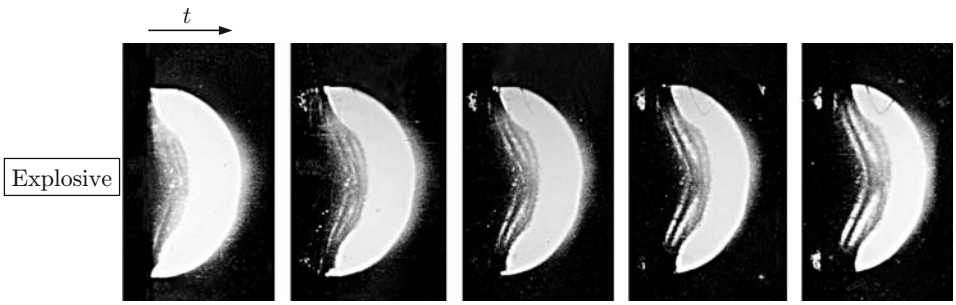

Fig. 3. High-speed photographic record of spall formation.

one can see the significant displacement s of the free surface and an increase in the scattered laser beam intensity I in the cavitation zone, which indicates intense development of cavitation. The displacement reaches a maximum in approximately 50 μsec from the moment of reflection of the incident pulse. From Fig. 2b, it follows that the mass-velocity jump corresponds to the beginning of free-surface displacement [7]. In this case, high-speed records do not show spalls in the cavitation zone.

The occurrence of spalls was first recorded in experimental studies of the structure of high-velocity flows resulting from low-depth underwater explosions [8]. High-speed recording has made it possible to observe the formation of a number of cavitating spall layers in the late stages of cavitation development (Fig. 3). In Fig. 3, the explosive charge is at the left and the free surface is located vertically.

As is known, the occurrence of spalls is characteristic of the brittle rupture of free-surface solids under shock-wave loading. Several spalls appear when the shock-loading parameters allow a system of cracks to be formed successively by the mechanism of occurrence of critical tensile stresses. However, as noted above, the critical tensile stress in a liquid is an obscure notion, the more so as the layers have a foam-like structure. The question arises: What causes the development of cracks in a cavitating liquid and are the properties of such liquids similar to the properties of a solid under brittle fracture? An answer to this question depended on the understanding of the dynamics of the state of liquids in the late stages of cavitation development, in which the structure of the cavitating liquid becomes close to the structure of the foam. In fact, the answer was obtained in experimental studies of the mass velocity profile in the zone of intensely developing cavitation, which showed that the profile remained unchanged in the cavitation zone [9]. This finding, which was called the frozen mass-velocity field effect, underlies the combined two-phase mathematical model, which allows numerical investigation of the dynamics of the sate of a liquid under shock-wave loading up to a state close to fracture.

This model, in particular, has made it possible to obtain an analytical solution of the problem of the dynamics of the average density in the cavitation zone in a simplified formulation with the assumption of instantaneous relaxation of tensile stresses behind the rarefaction wave front [10]. A drawback of this approximation was that the mass velocity field was determined from the profile of the shock wave incident on the free surface ignoring the fact that the rarefaction-wave profile varied significantly during cavitation development. However, this dynamically varying tensile stress field determines the mass velocity profile, which, in turn, determines the cavitation development in the late stages of liquid fracture under shock-wave loading.

The formulation of the problem proposed in the present paper allows investigation of the transformation of the rarefaction wave and its effect on the structure of cavitation zones near the free surface.

Formulation of the Problem. The problem of the wave structure arising in a liquid layer upon reflection of a piston-generated ultrashort shock wave from the free surface was studied in a one-dimensional formulation using the IKW model [11–13]. The so-called real liquid, i.e., a liquid containing natural microheterogeneities was studied. In this model, the conservation laws are written for the averaged pressure p, the density of the medium ρ, and the mass velocity u; in Lagrangian mass coordinates, they have are written as

$$\frac{\partial u}{\partial t} = \frac{1}{\rho}\frac{\partial p}{\partial \xi}, \qquad \frac{1}{\rho} = \frac{1}{\rho_0}\frac{\partial x}{\partial \xi}, \qquad \frac{\partial x}{\partial t} = u \tag{1}$$

(x and ξ are the Eulerian and Lagrangian coordinates, respectively, and ρ_0 is the density of the liquid).

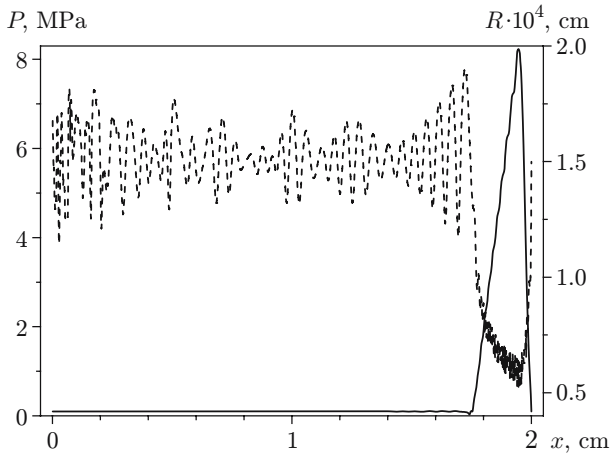

Fig. 4

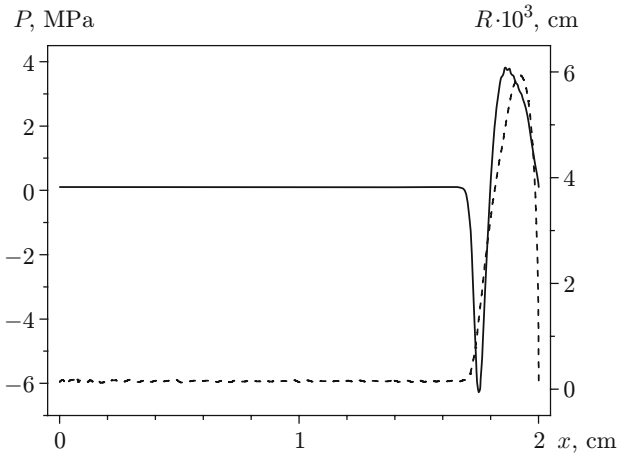

Fig. 5

Fig. 4. Bubble-radius distribution along the coordinate x (dashed curve) and the shock-wave profile (solid curve) before its reflection from the free surface ($t = 13$ μsec).

Fig. 5. Initial stage of formation of the rarefaction wave profile and the cavitation zone ($t = 15$ μsec): the solid curve is the pressure distribution over the layer thickness; the dashed curve is the bubble radius.

The conservation laws (1) are supplemented by a system of equations that describes the state of the medium and includes the Rayleigh equation for the dynamics of a single bubble of radius R in the liquid:

$$R\frac{\partial^2 R}{\partial t^2} + \frac{3}{2}\Big(\frac{\partial R}{\partial t}\Big)^2 = \frac{1}{\rho_l}\,(p_g - p), \tag{2}$$

the relations for ρ, R, and the gas-phase concentration k, and the equation of state for the bubble gas:

$$\rho = \rho_0(1-k), \qquad p_g = p_0(R/R_0)^{3\gamma}, \qquad k = k_0(R/R_0)^3. \tag{3}$$

Here ρ_l is the density of the liquid phase, p_g is the pressure in the bubbles, and p_0, R_0, and k_0 are the initial pressure, bubble radius, and gas-phase concentration in the bubble mixture, respectively. The compressibility of the liquid phase is described by the Tait equation [14], which, in view of (3), becomes

$$p = p_0 + \frac{\rho_0 c_0^2}{n}\Big[\Big(\frac{\rho}{\rho_0(1-k)}\Big)^n - 1\Big]. \tag{4}$$

System (1) was solved by the method described in [15] using an explicit difference scheme and linear and quadratic artificial von Neumann–Richtmyer artificial viscosities. The value of the artificial viscosity was chosen so as to smooth the pressure oscillations behind the shock-wave front due to the use of the numerical scheme with the steepness of the front being conserved. The Rayleigh equation (2) describing the dynamics of a single bubble was solved using a fourth-order Runge–Kutta–Merson method with an automatic choice of a step [16].

Calculation Results. Numerical analysis of the dynamics of the rarefaction wave structure and cavitation development was performed for a liquid layer of width l at an initial concentration (volumetric density) k_0 of nuclei of radius R_0. The initial perturbation in the form of a shock wave of triangular profile with an amplitude $p_{\max}$ and a pulse width τ was formed on the left boundary by the motion of the piston. Calculation results for $l = 2$ cm, $k_0 = 10^{-7}$, $R_0 = 1.5$ μm, $p_{\max} = 8$ MPa, $\tau = 1.5$ μsec are presented in Figs. 4–8.

Figure 4 shows the bubble-radius distribution and the shock-wave profile at the time $t = 13$ μsec when the shock wave reaches the free surface. The initial parameters of microheterogeneities k_0 and R_0 are extremely small, and the intense bubble oscillations behind the front of the incident shock wave (the dashed curve in Fig. 4) has little influence on the profile and amplitude of this wave during its motion over the layer to the free surface.

Figure 5 shows the initial stage of formation of the rarefaction-wave profile, whose amplitude is -6 MPa. Intense expansion of cavitation nuclei leads to fast (during 1 μsec) relaxation of tensile stresses behind the rarefaction wave front and the occurrence of a compression phase with an amplitude of about 4 MPa. In the cavitation zone

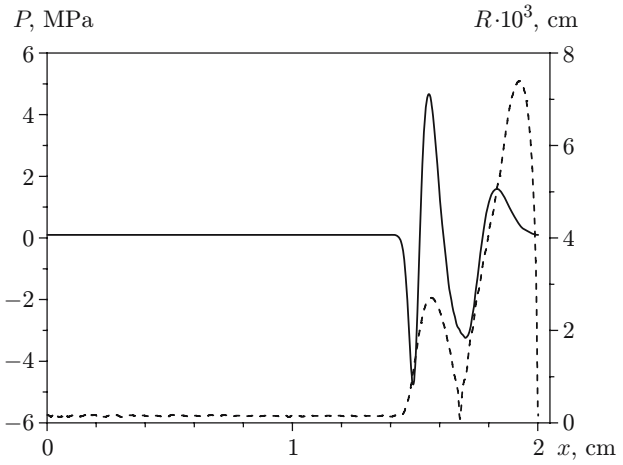

Fig. 6

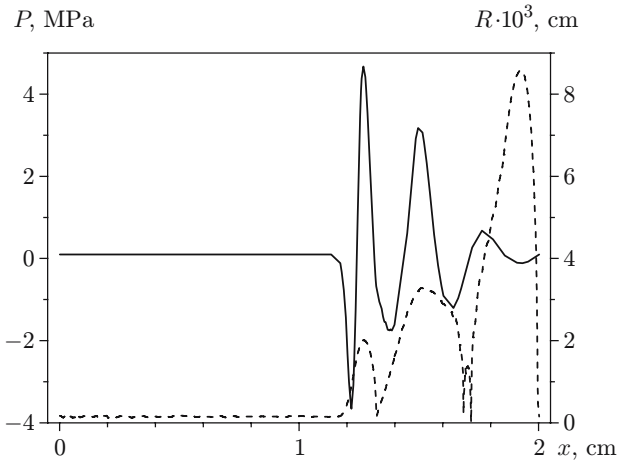

Fig. 7

Fig. 6. Formation of a double cavitation zone at $t = 16.7$ μsec (notation the same as in Fig. 5).

Fig. 7. Rarefaction wave in the form of a wave train with three cavitation zones at $t = 18.6$ μsec (notation the same as in Fig. 5).

(the dashed curve), the bubble radius exceeds the initial radius by a factor of 40. In the scale of the figure, the continuing bubble pulsations ahead of the rarefaction wave front are indistinguishable.

The further development of the cavitation process leads to the occurrence of alternating negative and positive pressure phases with fading amplitudes (Figs. 6 and 7). At $t = 18.6$ μsec, the rarefaction wave takes the form of a wave train, whose propagation into the depth of the liquid layer leads to the occurrence of three distinct zones (dashed curve in Fig. 7) with intensely growing bubbles located near the free surface and occupying about half the thickness of the liquid layer. In Fig. 7, it is evident that, under the adopted loading conditions, the cavitation bubbles develop most intensely in the first cluster, the nearest to the free surface. In an analysis of the fracture process (during the bubble growth in the cavitation zone), the main characteristic becomes the gas-phase volume concentration k; therefore, it is reasonable to represent the calculation results for the cavitation processes as the dynamics of distribution of the values of k for various times. This allows a better visualization of the fracture process. Indeed, at $t = 19.2$ μsec (Fig. 8), near the free surface, one can clearly see only the first of the three cavitation zones, in which the gas-phase volume concentration exceeds 2%, and, in the other two zones, it is almost 30 times lower.

At the time $t = 29.5$ μsec (Fig. 9), the wave train reaches the piston, is reflected from it, and begins to propagate in the opposite direction. It is evident that the tensile stress amplitude in the layer does not exceed -1 MPa, and in the main part of the layer (0.5 cm $\leqslant x \leqslant$ 2.0 cm), the pressure is nearly atmospheric. At the center of the cavitation zone, the gas-phase volume concentration reaches 5.5%. The further process should be calculated using the combination model [17], according to which the initial stage of cavitation development up to tensile-stress relaxation is calculated using the IKW model. As a result, according to experimental data [9], a quasistationary mass-velocity field is formed in the cavitation zone. This means that the pressure gradient in the equation for pulses can be ignored, and the constitutive system (1)–(4) is significantly simplified to

$$\frac{\partial}{\partial t}\Big(\frac{1}{\rho}\Big) = \frac{1}{\rho_0}\,\frac{\partial u}{\partial \xi}, \qquad \frac{\partial u}{\partial t} = 0, \qquad \frac{\partial x}{\partial t} = u, \qquad p = p_0, \qquad \frac{1}{\rho} = \frac{1}{\rho_{0,l}} + v_b$$

(p_0 is the initial pressure and v_b is the volume of cavitation bubble in unit mass of the mixture). Thus, the Rayleigh equation is omitted and the density of the mixture ρ becomes the main flow characteristic, which is uniquely related to the gas-phase volume concentration $k(x, t)$. Features of the given model are the absence of limitations on the bubble density and the possibility of calculating the dependence $k(x, t)$ in the case of unbounded increase in the gas-phase concentration.

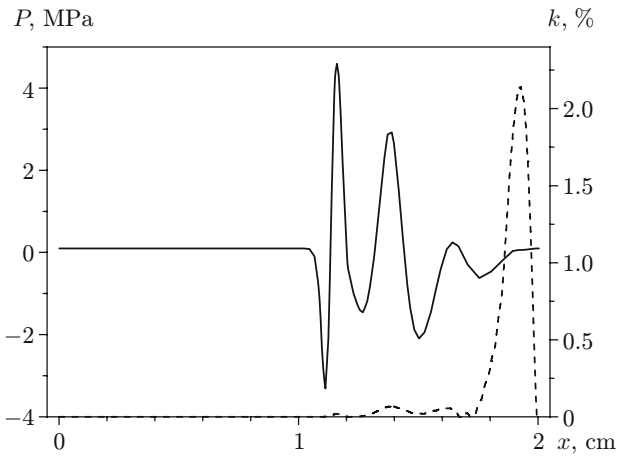

Fig. 8

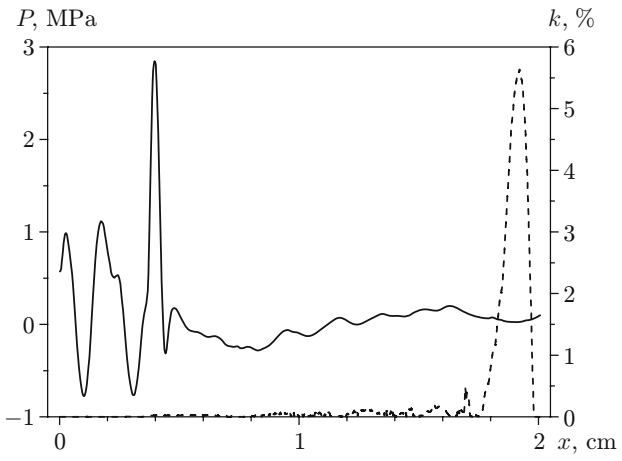

Fig. 9

Fig. 8. Distribution of the gas-phase pressure (solid curve) and volume concentration of the k (dashed curve) over the layer thickness at $t = 19.2$ μsec.

Fig. 9. Tensile-stress relaxation (solid curve) and volume concentration distribution (dashed curve) in the main part of the layer ($t = 29.5$ μsec).

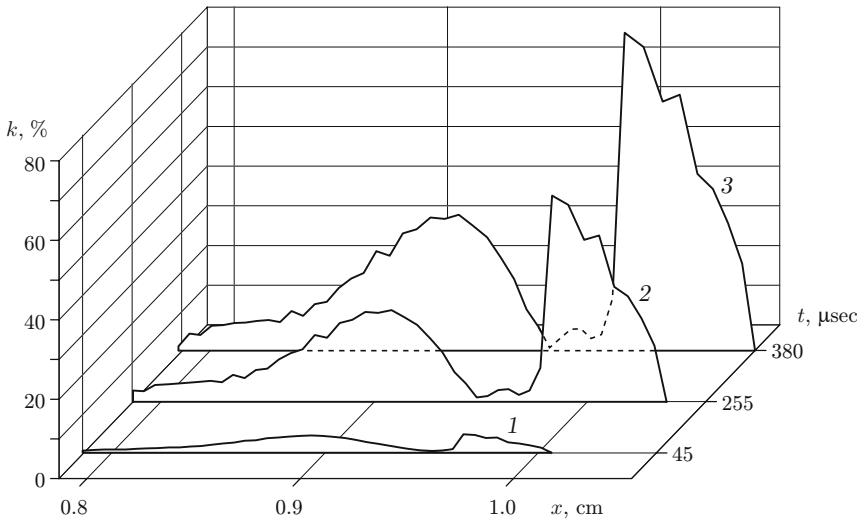

Fig. 10. Dynamics of formation of two spalls near the layer surface for $t = 45$ (1), 255 (2), 380 μsec (3).

Figure 10 gives results of a numerical analysis of the distribution $k(x, t)$ for three times [17]. The calculation was performed for a layer of thickness $l = 1$ cm and an incident bell-shaped pressure pulse of width $\tau = 1$ μsec with an amplitude equal to 5 MPa for the values of k_0 and R_0 indicated above. One can see two spall layers formed in a narrow zone (0.8 cm $\leqslant x \leqslant$ 1.0 cm) in the vicinity of the free surface, in which the maximum value of $k(x, t)$ reaches 80 and 30%, respectively. For comparison, Fig. 11 shows two frames of high-speed recording: the initial shape of the visible cavitation zone and the final, nearly foam-like, structure of the cavitating liquid flow with two spalls [17].

Conclusions. The two-phase nonequilibrium IKW model is suitable for one-dimensional numerical studies of the dynamics and mechanism of formation of a mass velocity field and cavitation zones in a liquid upon shock-pulse reflection from the free surface. The development of a system of cavitation zones with increasing gas-phase volume concentration near the free surface results from oscillations of the structure of the rarefaction-wave profile.

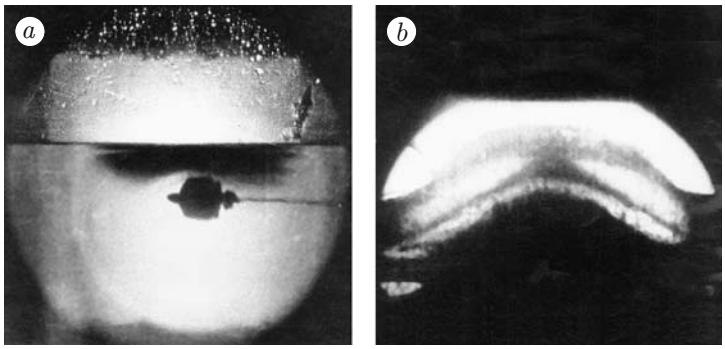

Fig. 11. High-speed records: (a) initial shape of the cavitation zone; (b) two cavitating spalls in the cavitation zone.

Upon completion of tensile stress relaxation, a quasistationary mass-velocity field is formed in the cavitation zone. This significantly simplifies the mathematical model and allows one to pass from the IKW model to the model of frozen mass-velocity field. The process of formation of the experimentally observed spall layers can ultimately be calculated using the combined model, which assumes almost unbounded bubble growth in the subsurface cavitating layers.

This work was supported by the Russian Foundation for Basic Research (Grant No. 06-01-00317), an integration project of the Siberian Division of the Russian Academy of Sciences 4.14.4, and the Programs of support of leading scientific schools of the Russian Federation (Grant NSh.-8583.2006.1).

REFERENCES

1. F. G. Hammitt, A. Koller, O. Ahmed, et al., "Cavitation threshold and superheat in various fluids," in: *Proc. of the Conf. on Cavitation* (Edinburgh, Sept. 3–5, 1974), Mech. Eng. Publ., London (1976), pp. 341–354.
2. M. Strasberg, "Undissolved air cavities as cavitation nuclei," in: *Cavitation in Hydrodynamics*, Nat. Phys. Lab., London (1956), pp. 1–13.
3. A. S. Besov, V. K. Kedrinskii, and E. I. Pal'chikov, "Optical-diffraction study of the initial stage of cavitation," *Pis'ma Zh. Tekh. Fiz.*, **10**, No. 4, 240–244 (1984).
4. G. I. Kanel', S. V. Razorenov, A. V. Utkin, and V. E. Fortov, *Shock-Wave Phenomena in Condensed Media* [in Russian], Yanus, Moscow (1996).
5. A. A. Bogach and A. V. Utkin, "Strength of water under pulsed loading stretching," *J. Appl. Mech. Tech. Phys.*, **41**, No. 4, 752–758 (2000).
6. V. K. Kedrinskii and S. I. Plaksin, "Rarefaction wave structure in cavitating liquid," in: *Proc. of the 11th IUPAP–IUTAM Int. Symp. on Nonlinear Acoustics* (Novosibirsk, August 24–28, 1987), Sib. Branch USSR Acad. Sci., Novosibirsk (1987), pp. 51–55.
7. A. S. Besov and V. K. Kedrinskii, "Dynamics of bubbly clusters and free surface at shock wave reflection," in: *Proc. of the 11th IUTAM Symp. on Bubble Dynamics and Interface Phenomena* (Birmingham, UK, September 6–9, 1993), Kluwer Acad. Publ. (1994), pp. 93–103.
8. V. K. Kedrinskii, "The experimental research and hydrodynamic models of a 'sultan'," *Arch. Mech.*, **26**, Nos. 3/4, 535–540 (1974).
9. A. R. Berngardt, "Dynamics of a cavitation zone under pulsed breakdown of water," in: *Dynamics of Continuous Media* (collected scientific papers) [in Russian], No. 104, Inst. of Hydrodynamics, Sib. Div., Russian Acad. of Sci., Novosibirsk (1992), pp. 3–15.
10. N. N. Chernobaev, "Cavitation development in rarefaction waves," *ibid.*, pp. 96–107.
11. S. V. Iordanskii, "On the equations of motion of a liquid containing gas bubbles," *Prikl. Mekh. Tekh. Fiz.*, No. 3, 102–110 (1960).
12. B. S. Kogarko, "On one model of a cavitating liquid," *Dokl. Akad. Nauk SSSR*, **137**, No. 6, 1331–1333 (1961).

13. L. Van Wijngaarden, "On the collective collapse of a large number of cavitation bubbles in water," in: *Proc. of the 11th Int. Congress of Appl. Mech.* (Munich, Germany, August 1964), Springer-Verlag, Berlin (1964), pp. 854–861.
14. V. K. Kedrinskii, *Hydrodynamics of Explosion: Experiment and Models* [in Russian], Izd. Sib. Otd. Ross. Akad. Nauk, Novosibirsk (2000).
15. A. A. Samarskii and Yu. P. Popov, *Difference Methods for Problems of Gas Dynamics* [in Russian], Nauka, Moscow (1980).
16. A. E. Mudrov, *Numerical Methods in BASIC, FORTRAN, and Pascal for Personal Computers* [in Russian], Rasko, Tomsk (1992).
17. M. N. Davydov and V. K. Kedrinskii, "Two-phase models of formation of cavitating spalls in a liquid," *J. Appl. Mech. Tech. Phys.*, **44**, No. 5, 660–666 (2003).